Inorg. Chem. **2008**, *47*, 4109−4117

A Versatile Series of Nickel(II) Complexes Derived from Tetradentate Imine/Pyridyl Ligands and Various Pseudohalides: Azide and Cyanate Compared†

Mohammad Habib,‡ Tapan K. Karmakar,‡ Guillem Aromí,*,§ Jordi Ribas-Ariño,|| Hoong-Kun Fun,⊥ Suchada Chantrapromma,# and Swapan K. Chandra*,‡

Department of Chemistry, Visva Bharati University, Santiniketan 731 235, India, Departament de Química Inorgànica, Universitat de Barcelona, Diagonal 647, 08028 Barcelona, Spain, Departament de Química Física and CERQT, Universitat de Barcelona, 08028 Barcelona, Spain, X-ray Crystallography Unit, School of Physics, Universiti Sains Malaysia, 11800 USM, Penang, Malaysia, and Department of Chemistry, Faculty of Science, Prince of Songkla University, Hat Yai, Songkhla 90112, Thailand

Received September 6, 2007

The chemical reactions of a family of tetradentate pyridyl/imine ligands, L1, L2, and L3 (L1 = [*N*,*N*′-bis(2-pyridinylmethylene)]ethane-1,2-diamine; L2 = [*N*,*N*′-bis(pyridin-2-yl)benzylidene]ethane-1,2-diamine; L3 = [*N*,*N*′-bis(2-pyridinylmethylene)]propane-1,3-diamine), with Ni^{II} in the presence of various pseudohalides (N_3^-, SCN^-, and NCO^-) have served to prepare six different complexes, $[Ni_2(L1)_2(N_3)_2](ClO_4)_2 \cdot H_2O$ (**1**), $[Ni_2(L2)_2(N_3)_2](ClO_4)_2$ (**2**), $[Ni_2(L2)_2(NCS)_4]$ (**3**), $[Ni_2(L2)_2(NCO)_2](ClO_4)_2$ (**4**), $[Ni_2(L3)_2(NCO)_2](ClO_4)_2$ (**5**), and $[Ni(L3)(N_3)_2]$ (**6**), which have been characterized by X-ray crystallography. Interestingly, four of these complexes are dinuclear and exhibit end-on (EO) pseudohalide bridges (**1**, **2**, **4**, and **5**), one is dinuclear and bridged exclusively by the tetradentate ligand (**3**), and one is mononuclear (**6**). The bulk magnetization of the complexes bridged by EO pseudohalides has been studied, revealing these ligands to mediate ferromagnetic coupling between the Ni^{II} ions, with modeled coupling constants, *J*, of +31.62 (**1**), +28.42 (**2**), +2.81 (**4**), and +1.72 (**5**) cm^{-1} (where the convention $H = -2JS_1S_2$ was used). The striking difference in the coupling intensity between N_3^- and NCO^- has prompted an investigation by means of density functional theory calculations, which has confirmed the experimental results and provided insight into the reasons for this observation.

1. Introduction

Pseudohalide ligands are major players in molecular magnetism. Among these, azide is undoubtedly the most extensively studied. Thus, a large number of coordination complexes have been prepared and studied with this ligand, both discrete[1] and polymeric.[2] The information ensued from this has served to establish magnetostructural correlations,[3,4] to identify various single-molecule magnets[5–9] or to unveil phenomena such as 1-D homometallic ferrimagnetism.[10] Although with less profusion than azide, the ligand thiocyanate has been relevant in the context of molecular magnetic materials, especially because it facilitates the occurrence of spin transition in iron systems.[11–13] On the contrary, the

† Dedicated to the memory of our beloved friend and great scientist Prof. Xavier Solans.

* To whom correspondence should be addressed. E-mail: guillem.aromi@qi.ub.es (G.A.), dr_swapan@sify.com (S.K.C.).
‡ Visva Bharati University.
§ Departament de Química Inorgànica, Universitat de Barcelona.
|| Departament de Química Física and CERQT, Universitat de Barcelona.
⊥ Universiti Sains Malaysia.
Prince of Songkla University.

(1) Escuer, A.; Aromí, G. *Eur. J. Inorg. Chem.* **2006**, 4721–4736.
(2) Ribas, J.; Escuer, A.; Monfort, M.; Vicente, R.; Cortés, R.; Lezama, L.; Rojo, T. *Coord. Chem. Rev.* **1999**, *195*, 1027–1068.
(3) Karmakar, T. K.; Ghosh, B. K.; Usman, A.; Fun, H. K.; Riviere, E.; Mallah, T.; Aromí, G.; Chandra, S. K. *Inorg. Chem.* **2005**, *44*, 2391–2399.
(4) Tandon, S. S.; Thompson, L. K.; Manuel, M. E.; Bridson, J. N. *Inorg. Chem.* **1994**, *33*, 5555–5570.
(5) Ako, A. M.; Hewitt, I. J.; Mereacre, V.; Clerac, R.; Wernsdorfer, W.; Anson, C. E.; Powell, A. K. *Angew. Chem., Int. Ed.* **2006**, *45*, 4926–4929.
(6) Aromí, G.; Parsons, S.; Wernsdorfer, W.; Brechin, E. K.; McInnes, E. J. L. *Chem. Commun.* **2005**, 5038–5040.
(7) Bell, A.; Aromí, G.; Teat, S. J.; Wernsdorfer, W.; Winpenny, R. E. P. *Chem. Commun.* **2005**, 2808–2810.

10.1021/ic701754u CCC: $40.75
Published on Web 04/11/2008

Scheme 1

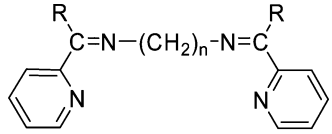

n=2, R=H; L1
n=2, R=Ph; L2
n=3, R=H; L3

ability of the pseudohalide cyanate to facilitate magnetic exchange has only been scarcely studied.[14–16] In this context, the differences or similarities between the ligands N_3^- and NCO^- as magnetic couplers have not been clearly established. In all cases, the structure of the products studied depends on the nature of the coligand used during the process of self-assembly. In this sense, we have been exploring the combination of azide with a family of flexible polydentate Schiff base ligands featuring pyridyl and imine functionalities (Scheme 1). Reactions with manganese(II) sources produced a series of polynuclear or dinuclear complexes exhibiting a variety of structural arrangements.[3,17] Some of these compounds served to propose the first magnetostructural correlation within dinuclear $[Mn^{II}_2]$ complexes bridged by two end-on (EO) μ-N_3^- groups.[3] The reactivity with Ni^{II} of the ligands in Scheme 1 is almost unexplored. Initial experiments of [*N*,*N*′-bis(pyridin-2-yl)benzylidene]ethane-1,2-diamine (L2) with $Ni(NO_3)_2$ and NaN_3 lead to the preparation of a ferromagnetically exchange-coupled cluster $[Ni_4(N_3)_8]$ (L2) with an $S = 4$ ground state.[18] These promising results have prompted us to investigate the reactivity of ligands [*N*,*N*′-bis(2-pyridinylmethylene)]ethane-1,2-diamine (L1), L2, and [*N*,*N*′-bis(2-pyridinylmethylene)]propane-1,3-diamine (L3) with $Ni(ClO_4)_2$ in the presence of N_3^-, SCN^-, or OCN^-. Interestingly, the results have been very diverse, and a series of various dinuclear or mononuclear complexes have been prepared and characterized. In particular, two new instances of extremely rare EO cyanato-bridged $[Ni_2]$ complexes will be presented. The structure and magnetic properties of the new complexes $[Ni_2(L1)_2(N_3)_2](ClO_4)_2$ (**1**), $[Ni_2(L2)_2(N_3)_2](ClO_4)_2$ (**2**), $[Ni_2(L2)_2(NCS)_4]$ (**3**), $[Ni_2(L2)_2(NCO)_2](ClO_4)_2$ (**4**), $[Ni_2(L3)_2(NCO)_2](ClO_4)_2$ (**5**), and $[Ni(L3)(N_3)_2]$ (**6**) are reported.

2. Experimental Section

Synthesis. Ethylenediamine, 1,3-diaminopropane, 2-benzoylpyridine, pyridine-2-carboxaldehyde, sodium azide, ammonium thiocyante, and sodium cyanate were purchased from Lancaster Chemical Co. Inc. and were used as received. All other solvents and chemicals were of analytical grade. Ligands L1−L3 (L1 = [*N*,*N*′-bis(2-pyridinylmethylene)]ethane-1,2-diamine; L2 = [*N*,*N*′-bis(pyridin-2-yl)benzylidene]ethane-1,2-diamine; L3 = [*N*,*N*′-bis(2-pyridinylmethylene)]propane-1,3-diamine) were prepared following the procedures reported previously[3,17] and gave satisfactory results upon elemental analysis.

$[Ni_2(L1)_2(N_3)_2](ClO_4)_2$ (1). To a methanolic solution (5 mL) of $Ni(ClO_4)_2 \cdot 6H_2O$ (0.183 g, 0.5 mmol) was added a solution of L1 (0.119 g, 0.5 mmol) in methanol (10 mL) over a period of 10 min. To the resulting dark-brown solution was added slowly an aqueous solution (2 mL) of NaN_3 (0.033 g, 0.5 mmol). The whole solution was then filtered, and the filtrate was left for slow evaporation. After 3−4 days, deep-red crystals of **1** were obtained (0.30 g, ∼66% yield), which were suitable for X-ray crystallography. These were collected by filtration and dried in vacuum. Anal. Calcd for $C_{28}H_{30}N_{14}O_9Cl_2Ni_2$ (**1**·H_2O): C, 37.57; H, 3.37; N, 21.91; Ni, 13.13. Found: C, 37.60; H, 3.25; N, 21.90; Ni, 13.10. IR (cm^{-1}): 2054, 1637, 1595, 1089, 622.

$[Ni_2(L2)_2(N_3)_2](ClO_4)_2$ (2). To an acetonitrile solution (5 mL) of $Ni(ClO_4)_2 \cdot 6H_2O$ (0.183 g, 0.5 mmol) was added L2 (0.195 g, 0.5 mmol) in acetonitrile (10 mL) over a period of 10 min. To the resulting brown solution was added slowly an aqueous solution (2 mL) of NaN_3 (0.033 g, 0.5 mmol). The solution was then filtered, and the filtrate was left for slow evaporation. After 3−4 days, red crystals of **2** were obtained (0.38 g, ∼64% yield). These were collected by filtration and dried in vacuum. Anal. Calcd for $C_{52}H_{44}N_{14}Cl_2O_8Ni_2$ (**2**): C, 52.87; H, 3.75; N, 16.60, Ni, 9.93. Found: C, 52.85; H, 3.74; N, 16.57; Ni, 9.90. IR (cm^{-1}): 2049, 1616, 1589, 1442, 1093, 620.

$[Ni_2(L2)_2(NCS)_4]$ (3). A solution of $Ni(ClO_4)_2 \cdot 6H_2O$ (0.183 g, 0.5 mmol) in 1:1 acetonitrile/methanol (10 mL) was added to a solution of L2 (0.195 g, 0.5 mmol) in 1:1 acetonitrile/methanol (10 mL) over a period of 10 min. A light-green solution was produced, which was warmed slightly and stirred for 5 min. The color of the solution became golden-yellow. To this was slowly added NH_4SCN (0.076 g, 1 mmol) dissolved in 1:1 acetonitrile/methanol, with constant stirring. The solution was then filtered and kept for slow evaporation. After 6 days, brown crystals of **3** were obtained (0.134 g, ∼60% yield), which were suitable for X-ray crystallography. These were kept in mother liquor because the compound was solvent-sensitive. Anal. Calcd for $C_{56}H_{47}N_{12}S_4Ni_2O_{0.75}$ (**3**·$1.5H_2O$): C, 58.70; H, 4.13; N, 14.67; Ni, 10.25. Found: C, 58.61; H, 4.09; N, 14.64; Ni, 10.21. IR (cm^{-1}): 2086, 2063, 1622, 1593.

$[Ni_2(L2)_2(NCO)_2](ClO_4)_2$ (4). A solution of $Ni(ClO_4)_2 \cdot 6H_2O$ (0.183 g, 0.5 mmol) in acetonitrile (5 mL) was added to a solution of L2 (0.195 g, 0.5 mmol) in acetonitrile (10 mL) over a period of 10 min. To the resulting red-brown solution was added slowly an aqueous solution (2 mL) of NaOCN (0.033 g, 0.5 mmol). The resulting mixture was then filtered, and the filtrate was left for slow evaporation. After 3−4 days, brown crystals of **4** were obtained (0.189 g, ∼65% yield), which were suitable for X-ray crystallography. These were collected by filtration and dried in vacuum.

(8) Boudalis, A. K.; Donnadieu, B.; Nastopoulos, V.; Modesto Clemente-Juan, J.; Mari, A.; Sanakis, Y.; Tuchagues, J.-P.; Perlepes, S. P. *Angew. Chem., Int. Ed.* **2004**, *43*, 2266–2270.

(9) Murugesu, M.; Habrych, M.; Wernsdorfer, W.; Abboud, K. A.; Christou, G. *J. Am. Chem. Soc.* **2004**, *126*, 4766–4767.

(10) Abu-Youssef, M. A. M.; Escuer, A.; Goher, M. A. S.; Mautner, F. A.; Reiss, G. J.; Vicente, R. *Angew. Chem., Int. Ed.* **2000**, *39*, 1624–1626.

(11) Bhattacharjee, A.; Ksenofontov, V.; Sugiyarto, K. H.; Goodwin, H. A.; Gutlich, P. *Adv. Funct. Mater.* **2003**, *13*, 877–882.

(12) Quesada, M.; Monrabal, M.; Aromí, G.; de la Peña-O'Shea, V. A.; Gich, M.; Molins, E.; Roubeau, O.; Teat, S. J.; MacLean, E. J.; Gamez, P.; Reedijk, J. *J. Mater. Chem.* **2006**, *16*, 2669–2676.

(13) Real, J. A.; Gaspar, A. B.; Muñoz, M. C. *Dalton Trans.* **2005**, 2062–2079.

(14) Arriortua, M. I.; Cortes, R.; Mesa, J. L.; Lezama, L.; Rojo, T.; Villeneuve, G. *Transition Met. Chem.* **1988**, *13*, 371–374.

(15) Clemente-Juan, J. M.; Mackiewicz, C.; Verelst, M.; Dahan, F.; Bousseksou, A.; Sanakis, Y.; Tuchagues, J. P. *Inorg. Chem.* **2002**, *41*, 1478–1491.

(16) Talukder, P.; Datta, A.; Mitra, S.; Rosair, G.; El Fallah, M. S.; Ribas, J. *Dalton Trans.* **2004**, 4161–4167.

(17) Karmakar, T. K.; Aromí, G.; Ghosh, B. K.; Usman, A.; Fun, H. K.; Mallah, T.; Behrens, U.; Solans, X.; Chandra, S. K. *J. Mater. Chem.* **2006**, *16*, 278–285.

(18) Karmakar, T. K.; Chandra, S. K.; Ribas, J.; Mostafa, G.; Lu, T. H.; Ghosh, B. K. *Chem. Commun.* **2002**, 2364–2365.

Table 1. Crystallographic Data for Complexes **1**−**6**

	1	**2**	**3**	**4**	**5**	**6**
formula	$Ni_2C_{28}H_{30}N_{14}O_9Cl_2$	$Ni_2C_{52}H_{44}N_{14}O_8Cl_2$	$Ni_2C_{56}H_{47}N_{12}O_{0.75}S_4$	$Ni_2C_{54}H_{44}N_{10}O_{10}Cl_2$	$Ni_2C_{32}H_{32}N_{10}O_{10}Cl_2$	$NiC_{15}H_{18}N_{10}O_{10}$
fw/g·mol^{-1}	894.98	1181.29	1145.72	1181.27	905.00	413.10
space group	*Cc*	$P2_1/n$	*P*1	$P2_1/n$	*Cc*	*Pbca*
a/Å	19.880(2)	10.3117(7)	12.8934(3)	10.2354(7)	19.6226(3)	15.2168(7)
b/Å	13.2773(16)	18.1579(13)	14.1523(3)	18.1502(13)	13.3588(3)	17.4383(8)
c/Å	14.2533(17)	28.747(2)	15.5819(3)	28.615(2)	14.9010(3)	13.3083(7)
α/deg	90	90	92.4880(10)	90	90	90
β/deg	110.9573(19)	99.387(2)	90.2890(10)	99.1680(10)	111.6160(10)	90
γ/deg	90	90	98.2270(10)	90	90	90
V/Å^3	3513.4(7)	5310.5(6)	2811.15(10)	5248.0(6)	3631.36(12)	3531.4(3)
Z	4	4	2	4	4	8
D_{calc}/g·cm^{-3}	1.692	1.477	1.354	1.495	1.655	1.554
F(000)	1832	2432	1186	2432	1856	1712
cryst size/mm	0.51 × 0.40 × 0.18	0.41 × 0.33 × 0.17	0.26 × 0.22 × 0.14	0.21 × 0.26 × 0.32	0.41 × 0.34 × 0.11	0.70 × 0.49 × 0.20
μ(Mo Kα)/mm^{-1}	1.298	0.878	0.868	0.889	1.256	1.129
T/K	100.0(1)	173	100.0(1)	293(2)	100.0(1)	100.0(1)
$2\theta_{max}$/deg	55.5	56.6	60.2	56.8	50.0	55.0
GOF	1.046	0.92	1.046	1.32	1.083	1.091
R; R_w	0.0944; 0.1964	0.0546; 0.1472	0.0854; 0.1256	0.0602; 0.2079	0.0922; 0.2342	0.0691; 0.1079
difference map max, min/e·Å^{-3}	+1.640, −0.716	+1.17, −0.73	+0.597, −0.551	+1.01, −0.93	+2.462, −0.815	+0.626, −0.453

Anal. Calcd for $C_{54}H_{44}N_{10}O_{10}Cl_2Ni_2$ (**4**): C, 54.90; H, 3.75; N, 11.85; Ni, 9.93. Found: C, 54.85; H, 3.70; N, 11.81; Ni, 9.91. IR (cm^{-1}): 2164, 1644, 1595, 1085, 624.

$[Ni_2(L3)_2(NCO)_2](ClO_4)_2$ (5). A solution of $Ni(ClO_4)_2·6H_2O$ (0.183 g, 0.5 mmol) in acetonitrile (5 mL) was added to a solution of L3 (0.126 g, 0.5 mmol) in acetonitrile (10 mL) over a period of 10 min. To the resulting red-brown solution was added slowly an aqueous solution (2 mL) of NaOCN (0.033 g, 0.5 mmol). The resulting mixture was then filtered, and the filtrate was left for slow evaporation. After 3−4 days, brown crystals of **5** were obtained (0.120 g, ∼70% yield), which were suitable for X-ray crystallography. These were collected by filtration and dried in vacuum. Anal. Calcd for $C_{32}H_{32}N_{10}O_{10}Cl_2Ni_2$ (**5**): C, 42.46; H, 3.56; N, 15.47; Ni, 12.97. Found: C, 42.40; H, 3.50; N, 15.45; Ni, 12.80. IR (cm^{-1}): 2177, 1643, 1596, 1085, 624.

$[Ni(L3)(N_3)_2]$ (6). A solution of $Ni(ClO_4)_2·6H_2O$ (0.183 g, 0.5 mmol) in acetone (5 mL) was added to a solution of L3 (0.126 g, 0.5 mmol) in acetone (10 mL) over a period of 10 min. To the resulting yellow hazy solution was added slowly an aqueous solution (2 mL) of NaN_3 (0.033 g, 0.5 mmol). The whole mixture was then filtered, and the filtrate was left for slow evaporation. After 3−4 days, reddish-brown crystals of **6** were obtained (0.100 g, ∼59% yield), which were suitable for X-ray crystallography. These were collected by filtration and dried in vacuum. Anal. Calcd for $C_{15}H_{18}ON_{10}Ni$ (**6**·H_2O): C, 43.60; H, 4.39; N, 33.91; Ni, 14.20. Found: C, 43.53; H, 4.24; N, 33.70; Ni, 14.11. IR (cm^{-1}): 2063, 1639, 1598, 1087, 627.

Caution! *Azido complexes and perchlorate salts are potentially explosive, especially in the presence of organic ligands. Therefore, these compounds must be handled with care and prepared only in small amounts.*

Physical Measurements. Elemental analyses for carbon, hydrogen, and nitrogen were performed using a Perkin-Elmer 2400II elemental analyzer. Nickel contents were determined gravimetrically as the nickel dimethylglyoximate complex. Variable-temperature magnetic susceptibility data were obtained with a Quantum Design MPMS5 SQUID spectrophotometer. Pascal's constants were utilized to estimate diamagnetic corrections to the molar paramagnetic susceptibility. IR spectra (as KBr pellets, 4000−400 cm^{-1}) were taken at 298 K using a Shimadzu model 8400 S spectrophotometer.

Crystal Structure Determinations and Refinement. Single crystals suitable for X-ray crystallographic analysis were selected following examination under a microscope. X-ray data for the complexes were collected with a Siemens SMART CCD diffractometer equipped with a graphite-monochromated Mo Kα radiation source ($\lambda = 0.710\,73$ Å). Intensity data were collected in the $\omega-2\theta$ scan mode. The data were corrected for Lorentz, polarization, and absorption effects, with the latter using *SADABS*.[18] The structures were solved by direct methods, and the structure solution and refinement was based on F^2. The non-H atoms were refined anisotropically. The aliphatic and aromatic H atoms have been calculated and refined using a riding model, whereas the amine H atoms where localized through difference synthesis. The H atoms of H_2O molecules could not be localized. The atomic scattering factors and anomalous dispersion terms were taken from the standard compilation.[19] All of the structures were solved with *SHELXS97* and refined with *SHELXL97* computer programs.[20,21] Crystal data and data collection details are collected in Table 1.

3. Results and Discussion

Synthesis. The tetradentate ligands L1−L3 were made by adopting reported procedures.[3,17] Thus, L1 or L2 could be easily obtained via the double condensation of ethylenediamine with pyridine-2-carboxaldehyde and 2-benzoylpyridine, respectively, in dehydrated ethanol. L3 could be prepared through the double condensation of 1,3-diaminopropane with pyridine-2-carboxaldehyde. The reaction of L1 with $Ni(ClO_4)_2·6H_2O$ and NaN_3 in aqueous methanol in a 1:1:1 molar ratio produced a dark-red crystalline complex of composition $[Ni_2(L1)_2(N_3)_2](ClO_4)_2·H_2O$ (**1**·H_2O). The same reaction with L2 in aqueous acetonitrile gave the analogous compound **2**. In both compounds, azide ions are behaving as EO bridging ligands. It is interesting to note that increasing the amount of N_3^- by up to 100% leads to the same compounds, **1** and **2**, respectively. Both complexes are insoluble in all common solvents. It must be emphasized here that the same reaction with L2 using $Ni(NO_3)_2$ had previously led to the formation of the tetranuclear complex $[Ni_4(N_3)_8]$

(19) *International Tables for Crystallography*; Kluwer Academic Publishers: Dordrecht, The Netherlands, 1992.
(20) Sheldrick, G. M.: *SHELXS97*; Universität Göttingen; Göttingen, Germany, 1997.
(21) Sheldrick, G. M.: *SHELXL97*; Universität Göttingen; Göttingen, Germany, 1997.

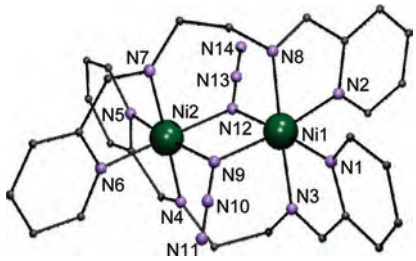

Figure 1. Representation of **1**. Only heteroatoms are labeled. H atoms are not shown for clarity.

(L2).[18] Because the only difference between the latter and the dinuclear complexes **1** and **2** is the counterion, this disparate reactivity must be caused by solubility or solid-state packing effects. If the pseudohalide NCO^- is made to play the role of N_3^- in the reaction of $Ni(ClO_4)_2 \cdot 6H_2O$ with L2, the resulting complex, compound **4**, has a structure analogous to that of complex **2**, featuring cyanate as the bridging ligand. However, if thiocyanate is used instead, the dinuclear compound **3** is formed where the pseudohalide only acts as a terminal ligand. When the more flexible ligand L3 was used, the results were also diverse. Thus, the reaction of $Ni(ClO_4)_2 \cdot 6H_2O$ with L3 and NaN_3 (molar ratio 1:1:1) produces the mononuclear complex $\mathbf{6} \cdot H_2O$. Formation of a mononuclear complex with L1 or L2 is precluded by the lack of flexibility of these ligands. The same reaction with NaOCN, however, results again in a dinuclear complex, compound **5**. The structural diversity observed with complexes **1**−**6** is not affected by the stoichiometry of the reactants because in all cases various molar ratios led to the same results described above.

IR Spectroscopy. All of the complexes except **3** and **6** are cationic in nature, having ClO_4^- as the counteranion. The stretching vibrations of ClO_4^- for these cationic complexes are found within the ranges 1085−1090 and 620−627 cm^{-1}. The IR spectra of **1**, **2**, and **6** exhibit bands at 2054 cm^{-1}, at 2049 cm^{-1}, and at 2061 cm^{-1}, respectively, corresponding to the asymmetric stretching vibrations of the ligand N_3^-, which are similar to those previously reported.[22,23] The asymmetric stretching vibrations of the ligand NCO^- for complexes **4** and **5** are found at 2165 and 2177 cm^{-1}, respectively. The IR spectrum of **3** exhibits bands corresponding to the asymmetric stretching vibrations of the ligand NCS^- at 2086 and 2063 cm^{-1}. The stretching vibrations of the C═N bond of the Schiff base L1 are located at 1637 and 1595 cm^{-1}, respectively. The stretching vibrations of the C═N bond of the Schiff base L2 are located at 1616, 1589, and 1442 cm^{-1}, respectively, while for the Schiff base L3, these are found at 1639, 1596, and 1440 cm^{-1}.

Description of the Structures. The structures of complexes **1**−**6** are represented in Figures 1−6. Crystallographic data are collected in Table 1, whereas selected parameters are given in Tables 2−7.

$[Ni_2(L1)_2(N_3)_2](ClO_4)_2 \cdot H_2O$ ($\mathbf{1} \cdot H_2O$). Compound **1** is a salt composed of a $[Ni^{II}_2]$ complex dication (Figure 1) and two ClO_4^- anions. The octahedral Ni^{II} centers are 2-fold-chelated (in cis fashion) and linked by two tetradentate ligands, L1, and bridged by two *cis*-EO μ-N_3^- groups, thereby featuring a very slightly distorted (see below) octahedral NiN_6 coordination environment. There is no clear difference between the metal bond distances to the pyridyl N atoms [in the 2.060(7)−2.077(6) Å range] and that to the imine N donor [range of 2.052(6)−2.077(6) Å]. The Ni−N distances to azide are in the range of 2.071(7)−2.103(6) Å. The azide groups are responsible for holding both metals in close proximity to each other [3.094(1) Å]. In this complex, the multidentate ligands L1 are surrounding the metal centers in a helical manner (Scheme 2). In turn, the bridging azido ligands are almost parallel to the planar core of the dimer. These two features confer the cluster idealized D_2 symmetry.

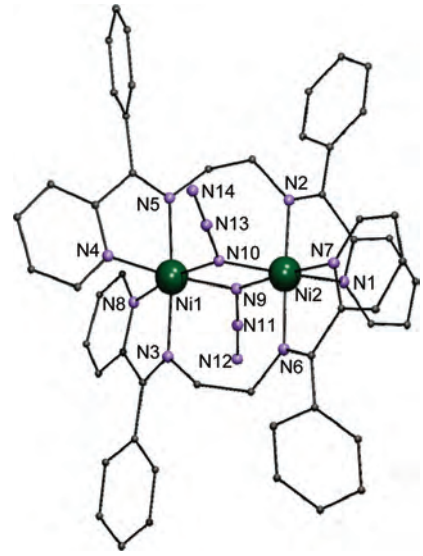

Figure 2. Representation of **2**. Only heteroatoms are labeled. H atoms are not shown for clarity.

Table 2. Selected Interatomic Distances (Å) and Bond Angles (deg) for **1**

Ni1−N1	2.072(6)	Ni1−N2	2.060(7)
Ni1−N3	2.080(6)	Ni1−N8	2.068(7)
Ni1−N9	2.071(7)	Ni1−N12	2.075(6)
Ni2−N4	2.076(7)	Ni2−N5	2.074(7)
Ni2−N6	2.077(6)	Ni2−N7	2.052(6)
Ni2−N9	2.077(8)	Ni2−N12	2.103(7)
Ni1···Ni2	3.094(1)	N9−N10	1.177(9)
N13−N12	1.181(9)	N10−N11	1.15(1)
N13−N14	1.14(1)		
N9−N10−N11	177.5(8)	N12−N13−N14	177.6(9)
N1−Ni1−N2	92.2(2)	N1−Ni1−N8	97.9(3)
N2−Ni1−N8	79.6(3)	N2−Ni1−N9	89.6(3)
N8−Ni1−N9	86.2(3)	N1−Ni1−N9	175.7(3)
N2−Ni1−N12	172.4(3)	N8−Ni1−N12	95.3(3)
N1−Ni1−N12	94.0(2)	N9−Ni1−N12	84.4(3)
N2−Ni1−N3	97.9(2)	N8−Ni1−N3	177.4(3)
N3−Ni1−N1	81.4(3)	N3−Ni1−N9	94.5(3)
N3−Ni1−N12	87.2(2)	N7−Ni2−N5	97.5(3)
N7−Ni2−N6	81.4(3)	N5−Ni2−N6	94.7(2)
N7−Ni2−N4	177.5(3)	N5−Ni2−N4	80.0(3)
N6−Ni2−N4	98.1(3)	N7−Ni2−N9	96.8(2)
N5−Ni2−N9	89.4(3)	N6−Ni2−N9	175.8(3)
N4−Ni2−N9	83.9(3)	N7−Ni2−N12	84.6(3)
N5−Ni2−N12	172.8(3)	N6−Ni2−N12	92.4(2)
N4−Ni2−N12	97.9(3)	N9−Ni2−N12	83.6(2)
Ni1−N9−Ni2	96.5(3)	Ni1−N12−Ni2	95.5(3)

(22) Barandika, M. G.; Cortes, R.; Lezama, L.; Urtiaga, M. K.; Arriortua, M. I.; Rojo, T. *J. Chem. Soc., Dalton Trans.* **1999**, 2971–2976.
(23) Cortes, R.; Delarramendi, J. I. R.; Lezama, L.; Rojo, T.; Urtiaga, K.; Arriortua, M. I. *J. Chem. Soc., Dalton Trans.* **1992**, 2723–2728.

Table 3. Selected Interatomic Distances (Å) and Bond Angles (deg) for **2**

Ni1−N3	2.084(3)	Ni1−N4	2.080(3)
Ni1−N5	2.073(3)	Ni1−N8	2.066(4)
Ni1−N9	2.093(4)	Ni1−N10	2.109(4)
Ni2−N1	2.076(4)	Ni2−N2	2.077(3)
Ni2−N6	2.071(3)	Ni2−N7	2.065(4)
Ni2−N19	2.086(4)	Ni2−N10	2.098(4)
Ni1···Ni2	3.138(1)	N10−N13	1.218(6)
N9−N11	1.210(6)	N13−N14	1.154(6)
N11−N12	1.154(6)		
N9−N11−N12	178.3(4)	N10−N13−N14	177.6(4)
N3−Ni1−N4	99.86(13)	N3−Ni1−N5	177.62(13)
N3−Ni1−N8	79.08(13)	N3−Ni1−N9	97.31(13)
N3−Ni1−N10	85.02(13)	N4−Ni1−N5	78.87(13)
N4−Ni1−N8	89.42(14)	N4−Ni1−N9	91.76(14)
N4−Ni1−N10	173.20(14)	N5−Ni1−N8	98.86(13)
N5−Ni1−N9	84.76(13)	N5−Ni1−N10	96.42(13)
N8−Ni1−N9	176.35(13)	N8−Ni1−N10	96.19(15)
N9−Ni1−N10	82.87(15)	N1−Ni2−N2	79.18(13)
N1−Ni2−N6	96.96(14)	N1−Ni2−N7	93.05(15)
N1−Ni2−N9	173.64(15)	N7−Ni2−N10	171.04(15)
N9−Ni2−N10	83.31(15)	N1−Ni2−N10	93.79(15)
N2−Ni2−N6	175.42(14)	N2−Ni2−N7	98.68(13)
N2−Ni2−N9	97.70(13)	N2−Ni2−N10	88.28(13)
N6−Ni2−N7	78.95(14)	N6−Ni2−N9	89.26(14)
N6−Ni2−N10	94.48(14)	N7−Ni2−N9	90.47(15)
Ni1−N9−Ni2	97.34(17)	Ni1−N10−Ni2	96.48(17)

$[Ni_2(L2)_2(N_3)_2](ClO_4)_2$ (2). Compound **2** is very similar to **1**. It also comprises two ClO_4^- anions that compensate for the charge of a cationic dinuclear complex of Ni^{II} (Figure 2), where the metals are chelated and connected by two tetradentate ligands, L2, and further bridged by two EO μ-N_3^- groups. Both metals display a slightly distorted NiN_6 octahedral environment and are maintained in close proximity to each other [3.138(1) Å], presumably by the action of the azido bridges. The Ni−N distances in this complex are not in statistically significant different ranges than those in **1** (Table 3). Here the ditopic ligands L2 are again attached to the metals in a helical fashion (Scheme 2), with the dimer also exhibiting noncrystallographic D_2 symmetry.

$[Ni_2(L2)_2(NCS)_4]\cdot 1.5H_2O$ ($3\cdot 1.5H_2O$). The unit cell of **3** consists of a pair of two chemically equal but crystallographically nonequivalent dinuclear complexes of Ni^{II}. Both units are neutral and centrosymmetric (Figure 3), comprising two distorted octahedral NiN_6 chromophores, where the metal ions are bridged and chelated by two tetradentate ligands

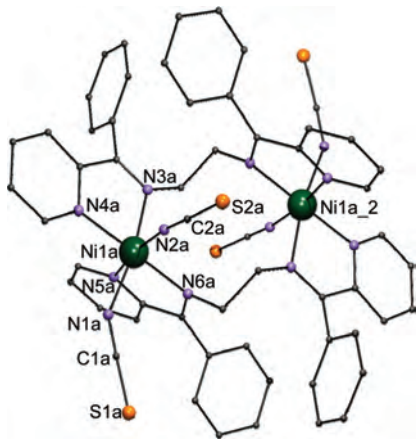

Figure 3. Representation of **3**. Only heteroatoms are labeled. H atoms are not shown for clarity.

Table 4. Selected Interatomic Distances (Å) and Bond Angles (deg) for **3**[a]

Ni1A−N1A	2.061(2)	Ni1A−N2A	2.048(2)
Ni1A−N3A	2.097(2)	Ni1A−N4A	2.113(2)
Ni1A−N5A	2.076(2)	Ni1A−N6A	2.139(2)
Ni1B−N1B	2.079(2)	Ni1B−N2B	2.044(2)
Ni1B−N3B	2.112(2)	Ni1B−N4B	2.099(2)
Ni1B−N5B	2.077(2)	Ni1B−N6B	2.129(2)
Ni1A···Ni1A*	5.565(1)	Ni2B···Ni2B*	5.518(1)
N2A−C2A	1.159(3)	N1B−C1B	1.167(6)
C2A−S2A	1.637(2)	C1B−S1B	1.627(3)
N1A−C1A	1.169(3)	N2B−C2B	1.161(3)
C1A−S1A	1.628(2)	C2B−S2B	1.631(3)
N2A−Ni1A−N1A	92.52(8)	N2A−Ni1A−N5A	87.81(8)
N1A−Ni1A−N5A	95.83(8)	N2A−Ni1A−N3A	93.02(8)
N1A−Ni1A−N3A	86.15(8)	N5A−Ni1A−N3A	177.81(8)
N2A−Ni1A−N4A	170.50(8)	N1A−Ni1A−N4A	87.32(8)
N5A−Ni1A−N4A	101.66(7)	N3A−Ni1A−N4A	77.50(7)
N2A−Ni1A−N6A	99.95(7)	N1A−Ni1A−N6A	165.23(8)
N5A−Ni1A−N6A	76.92(7)	N3A−Ni1A−N6A	100.93(7)
N4A−Ni1A−N6A	81.68(7)	N1A−C1A−S1A	178.1(2)
N2A−C2A−S2A	178.3(2)	N2B−Ni1B−N5B	89.32(8)
N2B−Ni1B−N1B	93.46(8)	N5B−Ni1B−N1B	95.10(8)
N2B−Ni1B−N4B	171.37(8)	N5B−Ni1B−N4B	98.84(8)
N1B−Ni1B−N4B	88.62(8)	N2B−Ni1B−N3B	94.05(7)
N5B−Ni1B−N3B	176.39(8)	N1B−Ni1B−N3B	86.01(8)
N4B−Ni1B−N3B	77.73(7)	N2B−Ni1B−N6B	94.82(7)
N5B−Ni1B−N6B	77.93(7)	N1B−Ni1B−N6B	169.09(8)
N4B−Ni1B−N6B	84.24(7)	N3B−Ni1B−N6B	100.46(7)
N1B−C1B−S1B	178.0(2)	N2B−C2B−S2B	177.9(2)

[a] Data including both (centrosymmetric) molecules, with labels A and B, respectively.

Scheme 2

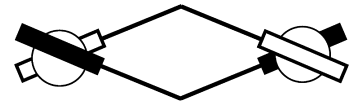

L2 and each are coordinated by two terminal NCS^- anions. Because the nickel centers are now only bridged by the ditopic ligands L2, the intermetallic separation [5.565(1) and 5.518(1) Å] is larger than that in the other dinuclear complexes. The Ni−N distances (to pyridyl or amine) are in a slightly longer range than those in complexes **1** and **2** [2.076(2)−2.139(2) Å]. The bonds of Ni to the N atom of

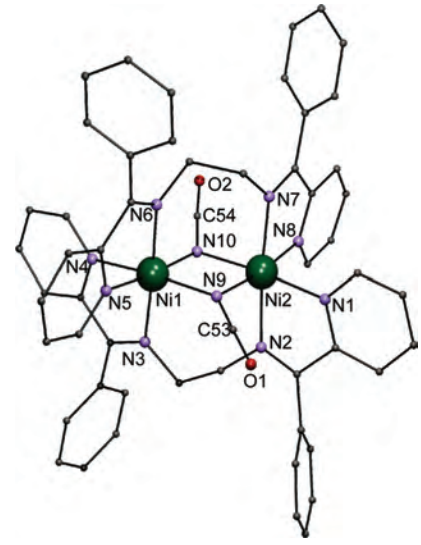

Figure 4. Representation of **4**. Only heteroatoms are labeled. H atoms are not shown for clarity.

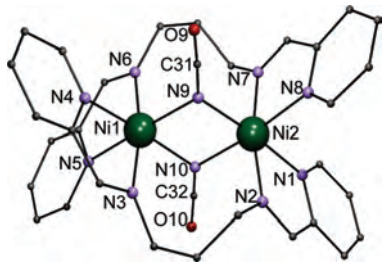

Figure 5. Representation of **5**. Only heteroatoms are labeled. H atoms are not shown for clarity.

Table 5. Selected Interatomic Distances (Å) and Bond Angles (deg) for **4**

Ni1−N3	2.066(3)	Ni1−N4	2.088(3)
Ni1−N5	2.066(3)	Ni1−N6	2.075(3)
Ni1−N9	2.079(3)	Ni1−N10	2.080(3)
Ni2−N1	2.070(3)	Ni2−N2	2.074(3)
Ni2−N7	2.060(3)	Ni2−N8	2.064(3)
Ni2−N9	2.115(3)	Ni2−N10	2.099(3)
Ni1···Ni2	3.100(1)	N10−C54	1.194(5)
N9−C53	1.195(5)	C54−O2	1.193(5)
C53−O1	1.199(5)		
N9−C53−O1	177.3(5)	N10−C54−O2	177.2(5)
N3−Ni1−N5	98.71(12)	N3−Ni1−N6	176.85(12)
N5−Ni1−N6	78.68(12)	N3−Ni1−N9	95.15(12)
N5−Ni1−N9	95.90(12)	N6−Ni1−N9	86.92(12)
N3−Ni1−N10	86.24(13)	N5−Ni1−N10	174.82(13)
N6−Ni1−N10	96.32(12)	N9−Ni1−N10	85.13(12)
N3−Ni1−N4	78.37(13)	N5−Ni1−N4	88.12(12)
N6−Ni1−N4	99.68(12)	N9−Ni1−N4	172.86(13)
N10−Ni1−N4	91.40(12)	N7−Ni2−N8	78.80(13)
N7−Ni2−N1	96.38(13)	N8−Ni2−N1	91.32(13)
N7−Ni2−N2	174.64(12)	N8−Ni2−N2	98.26(12)
N1−Ni2−N2	79.12(12)	N7−Ni2−N10	88.36(13)
N8−Ni2−N10	91.02(12)	N1−Ni2−N10	175.05(12)
N2−Ni2−N10	96.22(12)	N7−Ni2−N9	96.17(12)
N8−Ni2−N9	172.87(12)	N1−Ni2−N9	94.27(12)
N2−Ni2−N9	87.14(12)	N10−Ni2−N9	83.75(12)

thiocyanate range from 2.044(2) to 2.079(2) Å. These ligands coordinate the metals in a helical manner (as in Scheme 2).

$[Ni_2(L2)_2(NCO)_2](ClO_4)_2$ (4). Complex **4** (Figure 4) is analogous to **2**, with two bridging EO μ-NCO^- ligands instead of N_3^-. The small metric differences caused by changes in the pseudohalide are found in Tables 3 and 5, revealing no clearly identifiable trends. The bridging EO μ-NCO^- motif is extremely uncommon in coordination chemistry,[15,24–26] and, previously, it had been observed only in one Ni^{II} dinuclear compound.[14]

$[Ni_2(L3)_2(NCO)_2](ClO_4)_2$ (5). Complex **5** (Figure 5) is similar to complex **1**, with two bridging EO μ-NCO^- ligands instead of N_3^-, where the ditopic ligand now, L3, has one more $-CH_2-$ group separating the imine functions. This causes almost no structural changes on the core of the compound, although the NiN_6 coordination environment of the metal centers are now slightly more distorted as a result of the strain caused by the longer chain of L3 (see below). The structural consequences of changing the ligand also reflect

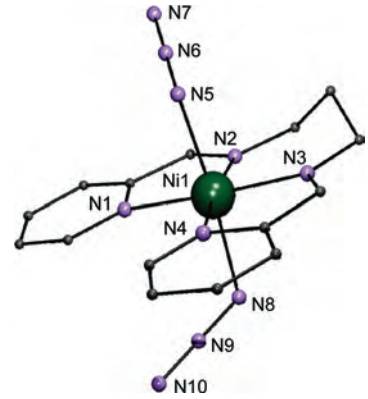

Figure 6. Representation of **6**. Only heteroatoms are labeled. H atoms are not shown for clarity.

Table 6. Selected Interatomic Distances (Å) and Bond Angles (deg) for **5**

Ni1−N3	2.081(9)	Ni1−N4	2.101(8)
Ni1−N10	2.104(9)	Ni1−N6	2.108(9)
Ni1−N9	2.115(8)	Ni1−N5	2.116(8)
Ni2−N2	2.045(9)	Ni2−N7	2.05(1)
Ni2−N1	2.065(7)	Ni2−N10	2.09(1)
Ni2−N8	2.094(8)	Ni2−N9	2.125(8)
Ni1···Ni2	3.112(1)	N10−C32	1.19(1)
N9−C31	1.18(1)	C32−O10	1.17(1)
C31−O9	1.19(1)		
N9−C31−O9	176.0(1)	N10−C32−O10	176.0(1)
N3−Ni1−N4	82.9(4)	N3−Ni1−N10	93.1(3)
N4−Ni1−N10	89.2(3)	N3−Ni1−N6	168.9(3)
N4−Ni1−N6	90.9(4)	N10−Ni1−N6	96.0(3)
N3−Ni1−N9	94.8(3)	N4−Ni1−N9	173.5(3)
N10−Ni1−N9	84.8(3)	N6−Ni1−N9	92.3(3)
N3−Ni1−N5	91.1(4)	N4−Ni1−N5	94.1(3)
N10−Ni1−N5	174.9(4)	N6−Ni1−N5	80.2(3)
N9−Ni1−N5	92.0(3)	N2−Ni2−N7	170.4(3)
N2−Ni2−N1	82.3(3)	N7−Ni2−N1	90.5(3)
N2−Ni2−N10	96.2(3)	N7−Ni2−N10	91.3(4)
N1−Ni2−N10	176.3(4)	N2−Ni2−N8	93.5(3)
N7−Ni2−N8	80.2(4)	N1−Ni2−N8	90.8(3)
N10−Ni2−N8	92.6(3)	N2−Ni2−N9	93.3(3)
N7−Ni2−N9	93.3(3)	N1−Ni2−N9	91.8(3)
N10−Ni2−N9	84.9(3)	N8−Ni2−N9	173.0(4)

on slightly longer Ni−N bonds [ranges of 2.090(10)−2.125(8), 2.065(7)−2.116(8), and 2.045(9)−2.108(9) Å for bonds to cyanate, pyridyl, and imine, respectively; see Table 6].

$[Ni(L3)(N_3)_2]\cdot H_2O$ ($6\cdot H_2O$). Complex **6** (Figure 6) is a neutral mononuclear complex of octahedral Ni^{II}, coordinated at the equatorial positions by the four N atoms of the ligand L3, with terminal N_3^- ligands at the axial positions. The fact that L3 can fold itself to coordinate one metal ion through its four donor atoms is a consequence of the larger flexibility provided by a central chain, longer than those in L1 and L2. The difference in nuclearity between **5** and **6** is more difficult to explain and may be due to solubility or packing effects. The ligand L3 in complex **6** is very flat, with all atoms but C8 within less that 0.1 Å from their least-squares plane (C8 being 0.73 Å away from that plane).

Continuous Shape Measures (CShMs). X-ray determinations revealed that all Ni^{II} ions in compounds **1**−**6** have a distorted NiN_6 octahedral environment. In most reports, the degree of distortion is only described with adjectives such as "slightly", "strongly", "severely", and so on. A numerical tool is necessary for an accurate quantitative description of

(24) Diaz, C.; Ribas, J.; El Fallah, M. S.; Solans, X.; Font-Bardia, M. *Inorg. Chim. Acta* **2001**, *312*, 1–6.
(25) El Fallah, M. S.; Escuer, A.; Vicente, R.; Badyine, F.; Solans, X.; Font-Bardia, M. *Inorg. Chem.* **2004**, *43*, 7218–7226.
(26) Mauro, A. E.; Klein, S. I.; Saldana, J. S.; Desimone, C. A.; Zukermanschpector, J.; Castellano, E. E. *Polyhedron* **1990**, *9*, 2937–2939.

Table 7. Selected Interatomic Distances (Å) and Bond Angles (deg) for **6**

Ni1−N2	2.045(2)	Ni1−N3	2.062(2)
Ni1−N8	2.109(2)	Ni1−N5	2.124(2)
Ni1−N4	2.130(2)	Ni1−N1	2.137(2)
N5−N6	1.199(3)	N6−N7	1.166(3)
N8−N9	1.201(3)	N9−N10	1.163(3)
N2−Ni1−N3	91.94(8)	N2−Ni1−N8	93.92(8)
N3−Ni1−N8	92.29(8)	N2−Ni1−N5	90.63(8)
N3−Ni1−N5	91.28(8)	N8−Ni1−N5	174.11(8)
N2−Ni1−N4	170.98(8)	N3−Ni1−N4	79.12(8)
N8−Ni1−N4	87.67(8)	N5−Ni1−N4	88.41(8)
N2−Ni1−N1	79.18(8)	N3−Ni1−N1	171.12(8)
N8−Ni1−N1	88.58(8)	N5−Ni1−N1	88.62(8)
N4−Ni1−N1	109.75(8)	N6−N5−Ni1	119.08(17)
N7−N6−N5	179.4(3)	N9−N8−Ni1	114.91(18)
N10−N9−N8	179.2(3)		

Table 8. Distance of the NiN_6 Coordination Polyhedron to the Perfect Octahedron for the Ni^{II} Ions of Complexes **1**−**6**, As Calculated by CShMs

complex; atom	CShM
1; Ni1	0.63
1; Ni2	0.76
2; Ni1	0.94
2; Ni2	0.78
3; Ni1a	1.39
3; Ni1b	0.97
4; Ni1	0.87
4; Ni2	0.78
5; Ni1	0.57
5; Ni2	0.52
6	1.11

the degree of distortion of the metal coordination geometry with respect to the ideal octahedron, other than going through the list of bonds and angles. CShMs fulfill this role perfectly and can be applied to any coordination geometry and with respect to any ideal polyhedron.[27] The CShM of a structure with respect to a given form is defined as a normalized mean-square deviation, in a 0−100 scale, of the actual polyhedron from the closest ideal polyhedron with that symmetry and shape. CShMs for Ni^{II} centers of all compounds reported in this paper have been calculated with respect to the ideal octahedron, and the distances are collected in Table 8. It is clear that the distortion from the perfect octahedron in all cases is not negligible (note, as a reference, that the exact intermediate geometry between the ideal octahedron and the ideal trigonal prism when going from one to the other through the Bailar twist is equidistant to both shapes at 4.42). From Table 8, a few conclusions might be drawn: (i) changing from ligand L1 to L2 does not affect significantly the distortion of the metal coordination geometry (as is seen by comparing **1** with **2**), (ii) bridging pseudohalides in these types of complexes seem to play a "template effect", preventing larger distortions from taking place (as is seen from the larger distortion of **3**), (iii) the structural effect in going from μ-N_3^- to μ-NCO^- is unappreciable (as is observed by comparing **2** and **4**), (iv) the additional $-CH_2-$ of L3 seems to help relax the distortion (see complex **5**), and (v) ligand L3 is not flexible enough to surround a lone metal ion without forming a significantly distorted mononuclear complex.

(27) Alvarez, S.; Avnir, D.; Llunell, M.; Pinsky, M. *New J. Chem.* **2002**, *26*, 996–1009.

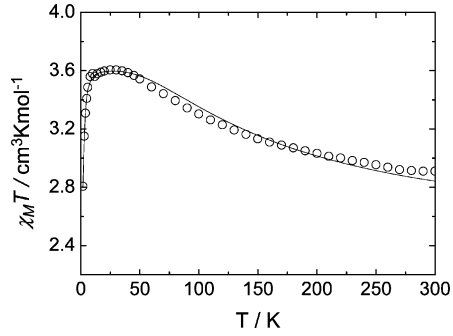

Figure 7. Plot of $\chi_M T$ vs T per mole of complex **1**, under a constant magnetic field. The solid line is a fit to the experimental data.

Table 9. Magnetic Parameters As Obtained from Simulation of the Experimental Data by a Full Diagonalization Fitting Procedure, or DFT Calculations, for Complexes **1**, **2**, **4**, and **5** (See the Text for Details)

complex	J(fit)[a]	J(DFT)[a]	D[a]	g
1	+32.0		4.7	2.19
2	+28.4	+30.8	3.2	2.19
4	+2.8	+6.7	3.6	2.23
5	+1.7		3.6	2.23

[a] In cm^{-1}.

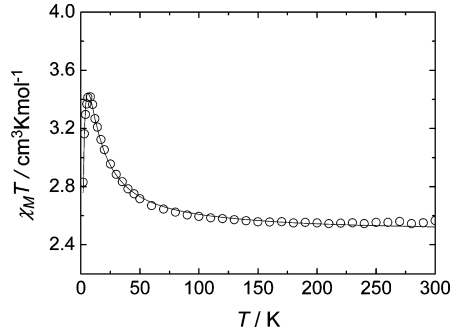

Figure 8. Plot of $\chi_M T$ vs T per mole of complex **4**, under a constant magnetic field. The solid line is a fit to the experimental data.

Table 10. Spin Densities on the Pseudohalide and Metals in Complexes **2** and **4**, Corresponding to Mulliken Population Analyses from DFT Calculations at the ROB3LYP[a] Level

	spin density	
atom (complex)	Mulliken	ROB3LYP
Ni (**2**)	1.617	1.671
donor N (**2**)	0.032	0.058
middle N (**2**)	−0.020	0.013
external N (**2**)	0.142	0.052
total N_3^- (**2**)	0.154	0.123
Ni (**4**)	1.637	1.689
donor N (**4**)	0.061	0.054
middle C (**4**)	0.028	0.028
external O (**4**)	0.037	0.022
total NCO^- (**4**)	0.126	0.104

[a] ROB3LYP is a DFT/B3LYP calculation where the orbital parts of the α and β orbitals are exactly the same (the calculation of J is carried out at the nonrestricted level; B3LYP). The restricted level is more convenient for qualitative discussions in terms of molecular orbitals.

Magnetic Properties. Variable-temperature bulk magnetization studies were performed in order to study the magnetic superexchange between Ni^{II} ions as mediated exclusively by EO azide or cyanate. Thus, susceptibility measurements under a constant magnetic field of 0.7 or 0.6 T were collected for complexes **1**, **2**, **4**, and **5** in the 2−300 K temperature range. The results are displayed in Figures 7 (representing the N_3^- compounds) and 8 (representing the NCO^- com-

pounds) in the form of $\chi_M T$ vs T plots (where χ_M is the molar paramagnetic susceptibility). For complexes **1/2**, the product $\chi_M T$ at 300 K is 2.91/2.89 cm^3 K mol^{-1} (slightly higher than that expected for two uncoupled Ni^{II} ions with $g = 2.2$; 2.42 cm^3 K mol^{-1}). This value increases steadily with cooling to reach a smooth maximum of 3.61/3.59 cm^3 K mol^{-1} at 25 K. To this follows a sharp decrease down to 2.80/2.89 cm^3 K mol^{-1} at 2 K. This shows that the coupling within both complexes is ferromagnetic. The low temperature decrease is ascribed to the effect of zero-field splitting (ZFS), although it might also be influenced by intermolecular interactions. The behavior of the cyanate complexes (**4/5**) is similar to that described above. In this case, the increase of $\chi_M T$ with cooling from room temperature ($\chi_M T$ at 300 K is 2.57/2.54 cm^3 K mol^{-1}) occurs at much lower temperatures, and then it takes place much more abruptly, resulting in a sharper maximum, now at 3.42/3.24 cm^3 K mol^{-1} at 8 and 6 K, respectively. The low temperature drop occurs down to 2.83/2.74 cm^3 K mol^{-1} at 2 K. The data were modeled by use of a numerical procedure based on the full diagonalization of the matrix arising from the spin Hamiltonian shown in eq 1.

$$H = -2JS_1S_2 + g\beta(S_1 + S_2) + 2\{D_{Ni}[S^2 - S_{Ni}(S_{Ni} + 1)/3]\} \quad (1)$$

In this Hamiltonian, the first term represents the magnetic coupling between the Ni^{II} centers of the dimer ($S_1 = S_2 = S_{Ni} = 1$), the second term is the Zeeman splitting of the dimer spin states, and the third term includes the effect of single-ion ZFS (D_{Ni}, which is equal for both Ni ions of each complex). The results of fitting the four sets of experimental data are collected in Table 9 in the form of parameters J, D_{Ni}, and g (see also Figures 7 and 8). The values obtained for the azide-bridged complexes are not surprising. It is well established that EO azide bridges mediate ferromagnetic coupling between Ni^{II} ions.[1,7,28] The coupling constants found within complexes **1** and **2** are indeed within the interval found for [Ni(μ-N_3)$_2$Ni] moieties.[29,30] Contrary to other metals, no correlation has been established yet for Ni^{II} relating the strength of the coupling and other structural parameters, although this possibility has been studied theoretically.[28] For the case of cyanate, the existing data in the literature are currently very scarce. In the only previous example with Ni^{II}, the EO μ-OCN^- has been shown to couple ferromagnetically both metals with a J value of 4.6 cm^{-1} (using the $H = -2JS_1S_2$ convention), similarly to compounds **4** and **5**. The striking fact is that, in similar circumstances, the group N_3^- leads to a coupling approximately 10 times stronger than the OCN^- ligand. The comparison is particularly appropriate when conducted between compounds **2** and **4**, which only differ in the nature of the pseudohalide bridge.

Density Functional Theory (DFT) Calculations. DFT calculations[31] were performed in order to get insights into the reasons why the coupling through azide is about 10 times stronger than that through cyanate. This was done on compounds **2** and **4**, which share almost exactly the same structure, with the only difference being the μ-N_3^- bridges in **2** versus the μ-OCN^- groups in **4**. For this, the B3LYP functional,[32] together with Ahlrichs' TZV basis set for the Ni ions,[33] and Ahlrichs' DZV basis set[34] for the rest of atoms were used. The J values were calculated in the same way as previously reported,[35] using the broken-symmetry approach to estimate the energy of the low-spin states. Given the fact that we are using the $H = -2JS_1S_2$ convention for the exchange Hamiltonian, the equation for calculating the J values is $J = [E(QT) - E(BSS)]/6$, where $E(QT)$ is the energy of the quintet state of the dinuclear Ni complex and $E(BSS)$ is the energy of its broken-symmetry singlet. The J values obtained from the calculation are 30.8 cm^{-1} for the azide bridge complex (**2**) and 6.7 cm^{-1} for the compound with OCN^- (**4**). The coincidence with the experimental values is quite satisfactory, with the overestimation being slightly more important for the latter (by 3.9 cm^{-1}) than for complex **2** (2.4 cm^{-1}). The error is thus more visible for complex **4** than for compound **2**. Despite the small deviations, the calculations unambiguously confirm the trends established by the experimental observations.

These results can be interpreted by comparing the representation of the singly occupied molecular orbitals (SOMOs) of **2** and **4** as obtained from these calculations, in particular the contribution made to these orbitals by the ligands azide and cyanate, respectively (Figure 9). The latter have been calculated at the ROB3LYP level and correspond to the quintet state. Of these orbitals, SOMOs 2 and 4 have essentially d_{z^2} character and have almost no presence on the bridging ligands, whereas SOMOs 1 and 3 (with marked $d_{x^2-y^2}$ character) are strongly delocalized on the atoms of azide or cyanate and are, therefore, those defining the nature of the superexchange. Inspection of SOMOs 1 and 3 reveals that the azide and cyanate contributions to these orbitals display rather different topologies. For example, the middle atom of the group N_3^- has almost zero contribution, while the C atom of OCN^- clearly participates in the form of a bonding π interaction with the N donor atom (SOMO 1). This is consistent with the composition of the highest occupied molecular orbitals (HOMOs) of the free ligands (as calculated by DFT methods; see the Supporting Information, Figure S1), which are the orbitals that interact with the metallic magnetic orbitals in the construction of the SOMOs.[36] Indeed, the HOMOs of the free ligands possess features similar to these exhibited by their contribution to

(28) Ruiz, E.; Cano, J.; Alvarez, S.; Alemany, P. *J. Am. Chem. Soc.* **1998**, *120*, 11122–11129.
(29) Sain, S.; Bid, S.; Usman, A.; Fun, H. K.; Aromi, G.; Solans, X.; Chandra, S. K. *Inorg. Chim. Acta* **2005**, *358*, 3362–3368.
(30) Vicente, R.; Escuer, A.; Ribas, J.; ElFallah, M. S.; Solans, X.; Fontbardia, M. *Inorg. Chem.* **1993**, *32*, 1920–1924.
(31) Frischm, M. J.; et al. *Gaussian 98, version A7*, Pittsburgh, PA, 1998.
(32) Becke, A. D. *J. Chem. Phys.* **1993**, *98*, 5648–5652.
(33) Schafer, A.; Huber, C.; Ahlrichs, R. *J. Chem. Phys.* **1994**, *100*, 5829–5835.
(34) Schafer, A.; Horn, H.; Ahlrichs, R. *J. Chem. Phys.* **1992**, *97*, 2571–2577.
(35) Ruiz, E.; Rodriguez-Fortea, A.; Cano, J.; Alvarez, S.; Alemany, P. *J. Comput. Chem.* **2003**, *24*, 982–989.
(36) Aebersold, M. A.; Gillon, B.; Plantevin, O.; Pardi, L.; Kahn, O.; Bergerat, P.; von Seggern, I.; Tuczek, F.; Ohrstrom, L.; Grand, A.; Lelievre-Berna, E. *J. Am. Chem. Soc.* **1998**, *120*, 5238–5245.

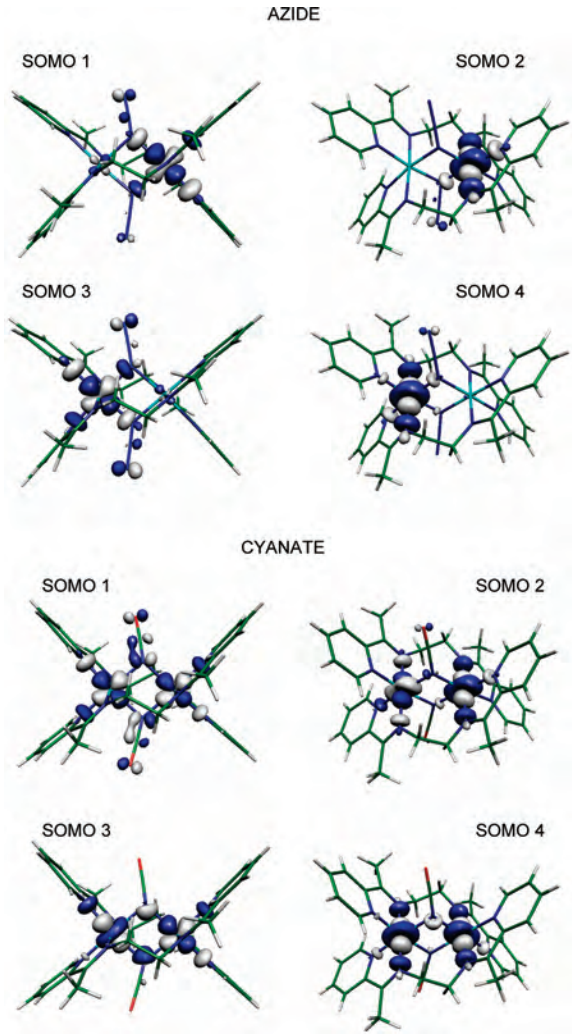

Figure 9. Representations of the SOMOs of the ferromagnetic state for complexes **2** and **4**, respectively, as calculated by DFT methods at the ROB3LPY level.

some of the SOMOs in Figure 9. Higher electronic density on the central C atom of NCO^- as compared to the central N atom of N_3^- can also be inferred from the simple Lewis structures of both species.

The highlighted differences between N_3^- and OCN^- affect significantly the magnitude of the overlap between the SOMOs. All SOMOs being orthogonal, the overlap integral must be zero, but the intensity of the ferromagnetic coupling is correlated with the overlap density between these orbitals. The topology of the contribution of the bridging ligands to the SOMOs causes this overlap density to be stronger for the N_3^- group than for the OCN^- ligand. Therefore, the electronic structures of the azide and cyanate groups clearly have a significant impact on the magnitude of the ferromagnetic coupling between both Ni^{II} centers. The calculated spin densities for the ground state (Table 10) confirm the lower participation to the SOMOs of the N_3^-'s central atom with respect to the central atom of OCN^-. This table also reveals that the total contribution to the spin density is slightly higher for azide than for cyanate. This also contributes to the stronger ferromagnetic coupling as mediated by the N_3^- bridge.

4. Concluding Remarks

The reactivity of a series of pyridine/imine-related ligands L1−L3 with $Ni(ClO_4)_2$ and the pseudohalides N_3^-, SCN^-, and NCO^- produces varied results, so far in the form of four dinuclear complexes bridged by azide or cyanate, one dinuclear species only supported by the polydentate ligands, and one mononuclear entity. The reasons for the exact structure isolated cannot be established unambiguously, and they are probably related to the solubility of the compounds and their ability to crystallize efficiently from a particular reaction system. CShMs can be used to quantify the degree of distortion of the Ni^{II} coordination sphere from a particular ideal polyhedron. In this manuscript, it appears because the change from N_3^- to NCO^- in analogous compounds causes no structural differences. Interestingly, this work has revealed clearly that, under identical circumstances, azide mediates ferromagnetic exchange 10 times more strongly than cyanate. DFT calculations are in agreement with these results. This theoretical study suggests that the cause for this is the electronic structure of the bridging ligands, which affects the composition of the SOMOs in this complex. Thus, in these orbitals, the contribution from the ligands translates into the presence of a π-bonding interaction between the central and donor atoms of NCO^-, which is not present in the SOMOs that contain the N_3^- ligand. This causes a decrease of the density of the overlap between the (orthogonal) SOMOs, thus diminishing the magnitude of the ferromagnetic contribution to the magnetic exchange.

Acknowledgment. We thank the Council of Scientific & Industrial Research (Scheme No. 01(2090)/06/EMR-II to S.K.C.) and the Department of Science and Technology (Scheme No. SR/S1/IC-12/2007 to S.K.C.) sponsored by the Government of India. We also thank the Malaysian Government and Universiti Sains Malaysia for research and the Spanish Ministry of Science and Technology ("Ramón y Cajal" research contract to G.A.). The University Grants Commission, New Delhi, India (for assistance under the DSA program and a teacher fellowship to T.K.K.), is also acknowledged.

Supporting Information Available: X-ray crystallographic file in CIF format for complexes **1**−**6** and representations of the MOs of the anions azide and cyanate as obtained through DFT calculations. This material is available free of charge via the Internet at http://pubs.acs.org.

IC701754U